ACS Sustainable Chemistry & Engineering

Research Article

Cite This: ACS Sustainable Chem. Eng. 2018, 6, 6146−6156

pubs.acs.org/journal/ascecg

Stacked Porous Iron-Doped Nickel Cobalt Phosphide Nanoparticle: An Efficient and Stable Water Splitting Electrocatalyst

Chaiti Ray,[†] Su Chan Lee,[†] Bingjun Jin,[‡] Aniruddha Kundu,[†] Jong Hyeok Park,[‡] and Seong Chan Jun*[,†]

[†]School of Mechanical Engineering, Yonsei University, 50 Yonsei-ro, Seodaemun-gu, Seoul 120-749, Republic of Korea

[‡]Department of Chemical and Biomolecular Engineering, Yonsei University, 50 Yonsei-ro, Seodaemun-gu, Seoul 120-749, Republic of Korea

Supporting Information

ABSTRACT: Exploration of proficient electrocatalyst from earth-abundant nonprecious metals in lieu of noble metal-based catalysts to obtain clean hydrogen energy through large-scale electrochemical water splitting is still an ongoing challenge. Herein, iron-doped nickel cobalt phosphide nanoplate arrays grown on a carbon cloth ($NiCoFe_xP$/CC) are fabricated using a simple hydrothermal route, followed by phosphorization. The electrochemical analysis demonstrates that the $NiCoFe_xP$/CC electrode possesses high electrocatalytic activity for water splitting in alkaline medium. Benefits from the synergistic effect between the metal centers, two-dimensional porous nanoplates, and unique three-dimensional electrode configuration of $NiCoFe_xP$/CC provide small overpotentials of 39 at 10 mA cm^{-2} and 275 mV at 50 mA cm^{-2} to drive the hydrogen evolution reaction and oxygen evolution reaction, respectively. Furthermore, the assembled two-electrode ($NiCoFe_xP$/CC‖$NiCoFe_xP$/CC) alkaline water electrolyzer can achieve 10 mA cm^{-2} current density at 1.51 V. Remarkably, it can maintain stable electrolysis over 150 h. The excellent activity and stability of this catalyst is proved to be a economical substitute of commercial noble metal-based catalysts in technologies relevant to renewable energy.

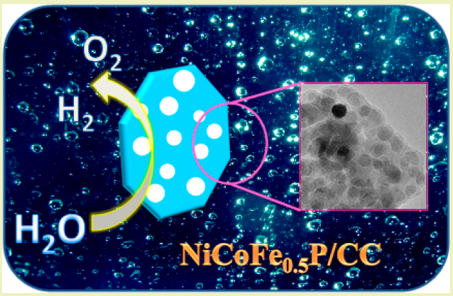

KEYWORDS: *Water splitting, Trimetallic phosphide, Uniform nanoplates, Low overpotential, Synergistic effects, Long-term stability*

INTRODUCTION

Hydrogen gas (H_2) is a well-known chemical product used at the global scale for various important industrial processes.[1,2] Developing efficient H_2 production technologies is very important and urgent for sustainable development for sustenance of human civilization due to the intrinsic advantages of the highest power density and zero carbon emissions for hydrogen energy. Electrochemical water splitting is a highly promising strategy for the conversion of intermittent renewable energy resources into high energy density hydrogen fuel to help overcome increasing energy consumption and combat environmental issues such as climate change.[3,4] To ensure efficient overall water splitting, an electrocatalyst should have significantly reduced overpotentials in both reactions. Nevertheless, water splitting in practical application is significantly limited by the slow kinetics of the oxygen evolution reaction (OER) and hydrogen evolution reaction (HER).[5,6] For example, the 1.8−2.0 V cell voltage, which is very large compared to the theoretical value of 1.23 V, is usually employed in commercial electrolyzers, necessitating effective catalysts to accelerate both half-cell reactions and reduce overpotentials.[7,8] The benchmark catalysts to split water are RuO_2 for OER and Pt/C for HER, both of which suffer from inadequacy and high expenditure.[9,10] In comparison to the well-investigated HER catalysis, the OER is more demanding, as it is both thermodynamically and kinetically challenging with involvement of four consecutive proton-coupled electron transfers and oxygen−oxygen bond formations. The HER and OER electrocatalysts usually can only perform well in different media. Thus, developing an electrocatalyst with high activity for HER and OER in the same electrolyte (either acidic or alkaline) can simplify systems and lower the costs.[11−13] In this respect, well-engineered catalysts prepared using earth-abundant elements such as Fe, Co, and Ni (and their derivatives) may offer affordable substitutes.[14−27]

Nickel-based chalcogenides such as Ni_3S_2,[28,29] $NiSe_2$,[30,31] NiO,[32] $Ni(OH)_2$,[33] NiB,[34] and Ni_2P[35] have received extensive attention as highly efficient HER and/or OER catalysts. Among them, nickel phosphide acquires many unique advantages because of its various nanostructures and physical properties.[7] In recent years, researchers have devoted their effort for the further enhancement of HER and OER activity of Ni_2P by tuning its structure and components, such as Mo-doped Ni_2P nanowires, Ni_5P_4 film, Ni_2P nanoparticles, and Ni_2P@C/G.[36−39] While binary phosphides have been explored as bifunctional electrocatalysts, improvements in catalytic per-

Received: December 20, 2017
Revised: March 8, 2018
Published: March 26, 2018

Downloaded via YONSEI UNIV on August 20, 2019 at 01:52:57 (UTC).
See https://pubs.acs.org/sharingguidelines for options on how to legitimately share published articles.

© 2018 American Chemical Society

DOI: 10.1021/acssuschemeng.7b04808
ACS Sustainable Chem. Eng. 2018, 6, 6146−6156

formance might be expected for ternary phosphides owing to synergistic effects.[40−43] Feng et al. performed a systematic study of the composition-dependent catalytic performance of $Ni_{2-x}Co_xP$ for water splitting.[44] Li et al. reported that NiCoP with hollow quasi-polyhedron structure exhibits better HER activity compared to CoP.[45] Again, as-prepared 3D nest-like NiCoP/CC by Du et al. have brilliant bifunctional catalytic performance toward water electrolysis.[14] In addition, previous experimental results have proved that iron-doping can not only increase the surface roughness but also expose the active sites of materials.[46] On the other hand, theoretical calculation demonstrated that Fe doping can also adjust the electronic structure of materials.[13] Both Li et al.[47] and Wang et al.[48] developed 3D Fe-doped Ni_2P nanosheet arrays on Ni foam as highly efficient bifunctional electrocatalysts for both HER and OER for improving efficiency of overall water splitting. Therefore, Fe-doping plays a crucial role toward the improvement of HER and OER activity as well as overall water splitting performance. Despite the significant progress achieved, the true active species in the OER catalysts based on metal chalcogenides, phosphides, and nitrides have been reported to be the oxidized species (oxides, hydroxides, and oxyhydroxides) on the material surface.[49,50]

Herein, we report our recent effort in designing and synthesizing a series of quaternary Fe-doped nickel cobalt phosphide nanoplate arrays supported on carbon cloth ($NiCoFe_xP$/CC) via a facile route for both the HER and OER in all pH (1−14) electrolyte. In particular, we found that the iron content has a significant influence on the catalytic activity. Among them, the $NiCoFe_{0.5}P$/CC as a binder-free electrocatalyst shows best HER activity with an overpotential of 39 mV vs RHE to achieve 10 mA cm^{-2} in alkaline medium. Simultaneously, this material also serves as an OER precursor in alkaline media. It was determined that the surface of $NiCoFe_{0.5}P$/CC would be transformed into Ni−Co−Fe hydroxide/oxyhydroxide as the active sites during the OER process, and the resulting catalyst displays an overpotential of 275 mV with an anodic current density of 50 mA cm^{-2}. An active phase uniformly deposited on a three-dimensional (3D) conductive framework provides better charge and mass transport efficiencies by facilitating rapid diffusion of both liquid reactants and gaseous products for water splitting. When $NiCoFe_xP$/CC was employed as both cathode and anode of alkaline medium water splitting, a current density of 10 mA cm^{-2} can be obtained at a cell voltage of 1.51 V with a long-term stability even after 150 h of electrolysis.

EXPERIMENTAL SECTION

Synthesis of $NiCoFe_xOH$/CC. First, a piece of carbon cloth (CC) (2 × 3 cm) was carefully activated using nitric acid treatment and then repeatedly rinsed with both ethanol and water. Then, the weight of pretreated CC was recorded. The $NiCoFe_xOH$/CC electrode was prepared by the following procedure: 10 mmol of urea, $Ni(NO_3)_2{\cdot}6H_2O$, $Co(NO_3)_2{\cdot}6H_2O$, and $Fe(NO_3)_3{\cdot}9H_2O$ with altered mole ratios of Ni/Co/Fe (1/1/0.1, 1/1/0.25, 1/1/0.5, and 1/1/1) were dispersed in 60 mL of deionized water to form a homogeneous solution. Then, the resultant solution and pretreated CC were transferred into a 100 mL Teflon-lined stainless steel autoclave and kept at 120 °C for 12 h. After naturally cooling to room temperature, the as-obtained $NiCoFe_xOH$/CC was washed with water and dried in vacuum at 60 °C for 6 h. For comparison, NiCo-hydroxide, CoFe-hydroxide, and NiFe-hydroxide/CC were also synthesized by the same hydrothermal process in the absence of Fe^{3+}, Ni^{2+}, and Co^{2+}, respectively.

Synthesis of the Phosphides. To prepare the phosphides, $NiCoFe_xOH$ precursor and $NaH_2PO_2{\cdot}H_2O$ (metal ion:P = 1:5) were put into a porcelain boat with NaH_2PO_2 at upstream position of the tube furnace. Subsequently, the samples were annealed at 300 °C for 1 h at 2 °C min^{-1} heating rate under 100 sccm Ar gas flow.

Structural and Surface Characterization. X-ray diffraction (XRD) patterns were acquired on a Bruker D8 Advance X-ray diffractometer with Cu Kα radiation (λ = 0.15406 nm). Raman spectroscopy was performed on a LabRam Aramis at Horiba Jovin Yvon. X-ray photoelectron spectroscopy (XPS) was performed in normal mode using a Kα (Thermo Scientific Inc. UK) XPS system with monochromatic Al Kα X-rays. All XPS spectra were corrected using the C 1s line at 284.6 eV followed by curve fitting and background subtraction. A JEOL-7800F field-emission scanning electron microscope (FESEM) was used to characterize the morphologies. Transmission electron microscopy (TEM) measurements were performed on a JEOL JEM-2010 electron microscope. High-resolution (HR)TEM and scanning (S)TEM analyses were performed using a JEM-ARM200F atomic resolution analytical microscope. To obtain the exact content of active materials in the different composites, inductively coupled plasma atomic emission spectroscopy (ICP-OES) was conducted using a PerkinElmer Optima 8300.

Electrochemical Studies. Electrochemical characterization and catalytic activity investigation of the different as-obtained electrodes were performed using a three-electrode system of a Ivium-n-Stat multichannel electrochemical analyzer, taking as-fabricated electrodes (1 cm^2) as a working electrode, a graphite rod as the counter electrode, and a Hg/HgO (in 1.0 M NaOH) as the reference electrode. All HER and OER performances of the electrocatalysts were evaluated by conducting linear sweep voltammetry (LSV) at a scan rate of 2 mV s^{-1} in 1.0 M KOH electrolyte. Electrochemical impedance spectroscopy (EIS) was recorded in a frequency range of 0.1 Hz−10 kHz with a sinusoidal voltage amplitude of 5.0 mV at bias potentials of −0.2 and 1.56 V (vs RHE) for the HER and OER, respectively. Chronopotentiometry curves were recorded at constant 10 mA cm^{-2} current density. All potentials reported in this paper were normalized with respect to an RHE by adding a value of (0.140 + 0.059 × pH) V. Overall water splitting activity was analyzed with a two-electrode system, using $NiCoFe_xP$/CC electrodes both as the cathode and anode in different pH electrolyte (acidic, neutral, and alkaline), and LSV curves were examined at a scan rate of 2 mV s^{-1}. The stabilities of the electrocatalysts were evaluated in a two-electrode fuel cell system for full water splitting using a 1.0 M KOH electrolyte at applied potentials of 1.51 and 1.70 V to reach initial catalytic current densities of 10 and 50 mA cm^{-2}, respectively.

RESULTS AND DISCUSSION

Morphology and Structural Analysis. Figure 1a displays schematic representation of the two-step synthetic strategy of novel $NiCoFe_xP$/CC with plate-like morphology. The first step is the hydrothermal reaction using CC as the substrate. After hydrothermal synthesis, the observed pink film on CC denotes the successful fabrication of hydroxide ($NiCoFe_xOH$/CC) material. The obtained hydroxide precursor was then used as the template for the synthesis of Fe-doped ternary Ni−Co−P ($NiCoFe_xP$) via direct phosphidation under an Ar atmosphere. During the annealing, NaH_2PO_2 would release PH_3,[51,52] which served as the phosphorus source to react with $NiCoFe_xOH$ precursor.

The X-ray diffraction (XRD) pattern of the $NiCoFe_xOH$/CC in Figure 1b represents no other diffraction peaks except the peaks of CC at 25.6° and 44°. This result directs to the amorphous nature of $NiCoFe_xOH$ nanoplates. Figure 1c shows XRD patterns of $NiCoFe_xP$/CC with Ni/Co/Fe feeding ratio of 1/1/0.5. The diffraction peaks for $NiCoFe_xP$ at 40.98°, 47.56°, 54.48°, and 75.42° are indexed as (111), (210), (300),

DOI: 10.1021/acssuschemeng.7b04808
ACS Sustainable Chem. Eng. 2018, 6, 6146−6156

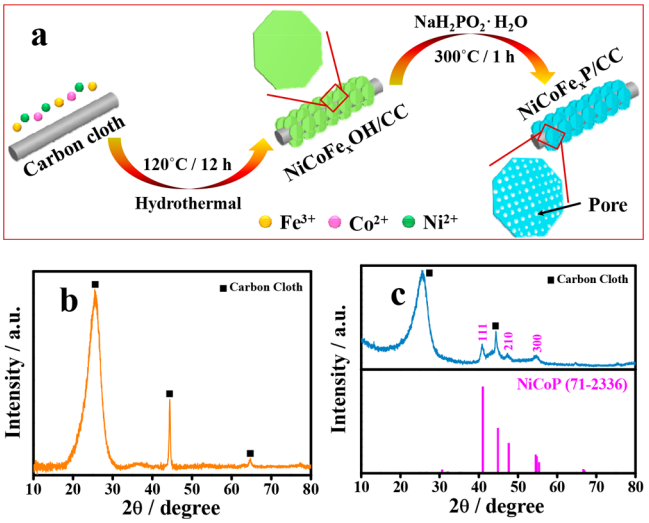

Figure 1. (a) Schematic illustration of the procedure for the synthesis of NiCoFe$_x$P/CC. XRD patterns of (b) NiCoFe$_x$OH and (c) NiCoFe$_x$P/CC nanostructures.

and (212) planes of hexagonal NiCoP (PDF no. 71-2336), respectively.[53] Note that no additional diffraction peaks of other Fe phases can be observed, suggesting that Fe is incorporated into the NiCoP lattices. The ICP-OES analysis of NiCoFe$_x$P scraped off from the CC with a Ni/Co/Fe feeding ratio of 1/1/0.5 exhibits that the atomic ratio of Ni:Co:Fe is 0.99:1:0.46 (Table S1), demonstrating the formation of the NiCoFe$_x$P nanostructure.

To study the chemical states of the elements in NiCoFe$_x$OH and NiCoFe$_x$P/CC, XPS analyses were performed. For NiCoFe$_x$OH, Ni 2p spectrum is well-fitted with two spin–orbit doublets (855.9 and 873.5 eV) as well as shakeup satellites (861.8 and 879.4 eV), characteristic for Ni^{2+} valence state (Figure S1a).[54,55] One extra peak at 857.1 eV is noticed, which corresponds to presence of Ni^{3+} in NiCoFe$_x$OH. The Co 2p XPS spectrum consists of one spin–orbit doublet and two shakeup satellites (Figure S1b). Deconvulated Co $2p_{3/2}$ spectrum represents the peaks for two different chemical environments for cobalt. The peaks at 781.1 and 782.9 eV are correspond to Co^{3+} and Co^{2+} ions, respectively.[56] It implies the coexistance of both the Co^{2+} and Co^{3+} species in fabricated

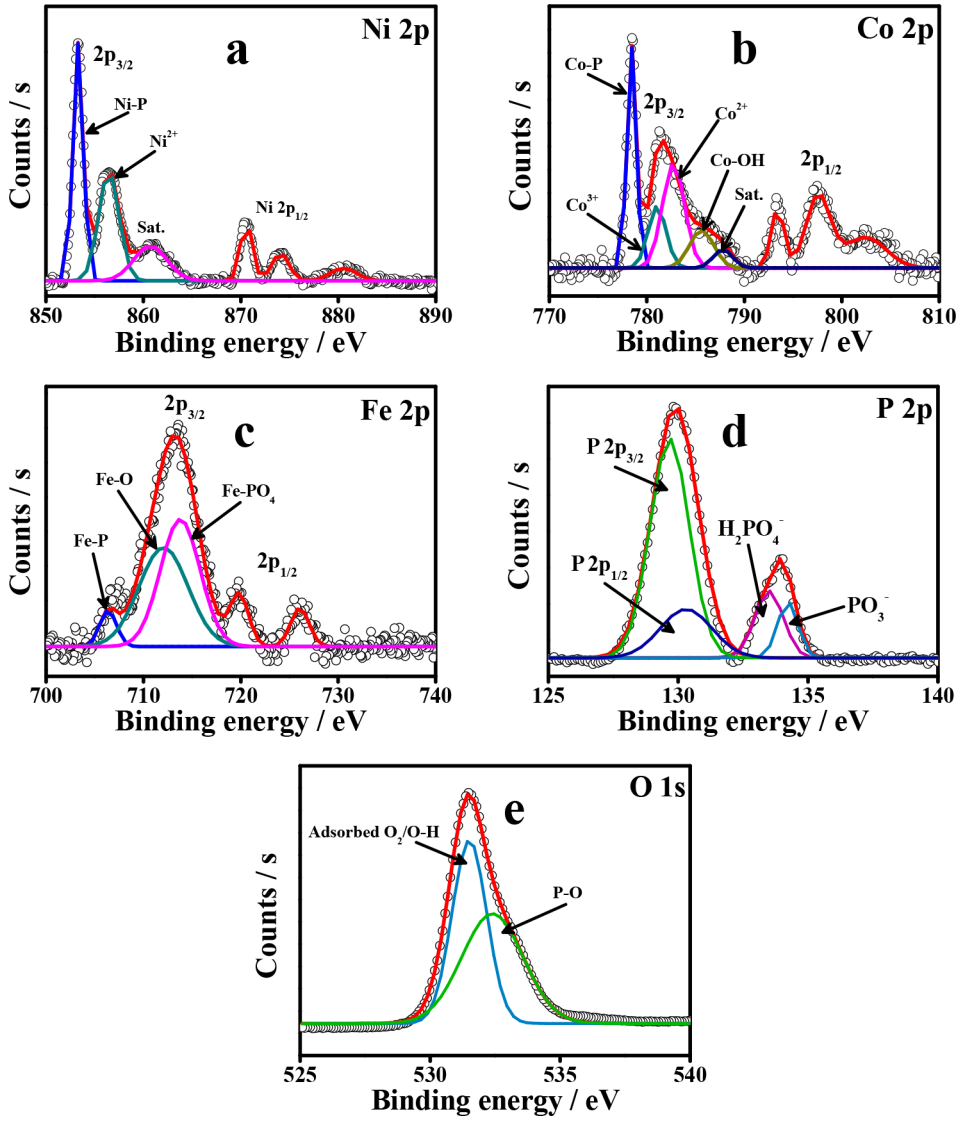

Figure 2. (a) Ni 2p, (b) Co 2p, (c) Fe 2p, (d) P 2p, and (e) O 1s XPS spectra of NiCoFe$_x$P/CC.

DOI: 10.1021/acssuschemeng.7b04808
ACS Sustainable Chem. Eng. 2018, 6, 6146–6156

hydroxide precursor. In Figure S1c, the peaks at binding energies of 712.6 and 726.0 eV are designated as Fe $2p_{3/2}$ and Fe $2p_{1/2}$ of Fe^{3+} oxidation state, respectively.[57] The XPS spectrum of O 1s region in $NiCoFe_xOH/CC$ as shown in Figure S1d indicates four oxygen peaks. The peaks at 531.03, 531.7, and 532.5 eV binding energies are characteristic peaks of Fe−O−H, Ni−O−H, and Co−O−H bonds.[58−61] The peak at 533.6 eV is appeared due to the physically or chemically adsorbed water molecule on the surface of $NiCoFe_xOH/CC$.[62] After thermal treatment with NaH_2PO_2, the surface chemistry of the resultant $NiCoFe_xP/CC$ is probed by XPS (Figure 2). As shown in Figure 2a, Ni $2p_{3/2}$ spectrum comprises of constituent peaks at 853.0 eV corresponding to Ni−P, as well as 856.3 and 860.8 eV come from oxidized Ni-based components because of surface oxidation.[63] The value of peak related to Ni−P is very close to metallic Ni (852.6 eV), suggesting the presences of partially charged Ni species ($Ni^{\delta+}$, $2 > \delta > 0$).[14] In the high-resolution Co $2p_{3/2}$ spectrum (Figure 2b), the peak traced at 778.4 eV is ascribed to Co−P bond. The peaks at 781.1 and 782.5 eV are attributed to Co^{3+} and Co^{2+} form of the oxidized cobalt species, respectively, while the peak at 785.6 eV is from the Co−OH bond.[64,65] The peak of Co 2p at 778.4 eV is shifted toward higher binding energy compared to that of Co metal (778.2 eV), which implies presence of cobalt in Co−P phase in partial positive charge ($Co^{\delta+}$).[14] The XPS spectrum of Fe $2p_{3/2}$ region (Figure 2c) has three peaks with corresponding binding energies at 713.5, 711.7, and 707.1 eV. The peak at 707.1 eV recommends the presence of reduced Fe species as Fe−P.[66] These reduced Fe species contain partial positive charge ($Fe^{\delta+}$, $0 < \delta < 2$), and the binding energy value is nearly same as that of metallic Fe (706.8 eV).[67] The observed peaks at 713.5 and 711.7 eV can be assigned to the oxidized Fe species formed on the sample surface, which could be associated with $FePO_4$ and Fe_2O_3, respectively.[67] The metallic features help to attain prompt electron transfer ability, robustness, and high tensile strength; hence, an effectual and sustainable electrocatalyst can be acquired. In Figure 2d, P 2p region clearly represents two different environments around P:metal phosphide (P $2p_{3/2=}$ 129.3 eV and P $2p_{1/2=}$ 130.1 eV) and oxidized phosphate species (133.9 eV).[68] The binding energy of P 2p at 129.8 eV is negatively shifted from that of elemental P (130.2 eV), which proposes partial negative charge (δ^-) on the P atom.[64] The peak at 133.9 eV is designated as oxidized form of P atoms resulting from surface oxidation of metal phosphide. The O 1s core level XPS spectra of $NiCoFe_xP$ (Figure 2e) can be deconvoluted in two peaks centered at 531.1 and 532.6 eV, which can be attributed to adsorbed oxygen and hydroxide species and P−O components, respectively. Therefore, it may be inferred that upon phosphorization, the catalyst surface becomes slightly phosphate functionalized.

FESEM image (Figure S1e) show that the CC is evenly covered with densely packed and vertically aligned $NiCoFe_xOH$ nanoplates. High-magnification FESEM image in Figure S1f shows smooth surface of hydroxide precursor. Figure 3a also supports dense packing of nanoplates over CC after phosphorization with retention of morphology. However, Figure 3b indicates rough surface of each nanoplate after thermal treatment. The elemental mapping of $NiCoFe_xP$ nanostructure (Figure 3c) reveals an even distribution of Ni, Co, Fe, and P elements. Further structural features were examined using TEM. The TEM image of $NiCoFe_xP$ (Figure 3d) shows that each nanoplate comprises numerous interconnected nanoparticles with disordered pores. The

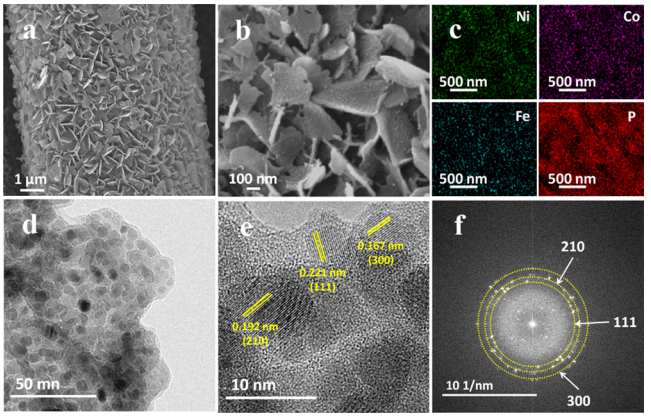

Figure 3. (a and b) FESEM images of $NiCoFe_xP/CC$ low and high magnifications, respectively. (c) Elemental mapping of $NiCoFe_xP/CC$ nanostructures showing Ni, Co, Fe, and P elements. (d) TEM image, (e) HRTEM image, and (f) corresponding SAED pattern of $NiCoFe_xP/CC$.

HRTEM image in Figure 3e shows well-resolved lattice fringes with *d*-spacing values of 0.22, 0.19, and 0.167 nm for the (111), (210), and (300) planes of NiCoP, respectively. This is also supported by several bright discrete spots in selected area electron diffraction (SAED) pattern (Figure 3f). Therefore, uniform $NiCoFe_xP$ nanostructures are fabricated on the CC, and Fe is incorporated as amorphous phosphide and oxide phases.

The as-synthesized Fe-doped nickel phosphide (NiFeP), Fe-doped cobalt phosphide (CoFeP), and nickel cobalt phosphide (NiCoP) on CC by following same reaction route in the absence of $Co(NO_3)_2$, $Ni(NO_3)_2$, and $Fe(NO_3)_3$, respectively, were also characterized with XRD and FESEM techniques (Figure S2).

Electrochemical Performance. The electrocatalytic performance of the as-prepared $NiCoFe_xP/CC$ for HER was evaluated in an alkaline electrolyte (1.0 M KOH) utilizing the typical three-electrode system. NiFeP, CoFeP, NiCoP, and commercial Pt−C (20 wt %) were also tested for comparison. Typical *iR*-corrected polarization curves in Figure 4a indicate poor HER performances of NiFeP, CoFeP, and NiCoP with large overpotentials of 109, 91, and 86 mV, respectively, at 10 mA cm^{-2} current density (η_{10}). In stark contrast, the $NiCoFe_xP$ electrode displays a very small η_{10} value of 39 mV, which is only 11 mV more than that of Pt−C (28 mV). More interestingly, $NiCoFe_xP$ provides a high current density (*j*) of 100 mA cm^{-2}, which is usually required for practical electrolysis,[69] with an η_{100} value (87 mV) close to that of Pt−C (75 mV), demonstrating promising future of $NiCoFe_xP$ for industrial applications. The corresponding *iR*-uncorrected polarization curves for all the tested electrocatalysts are shown in Figure S3. Figure 4b shows that the Tafel slope of $NiCoFe_xP$ is 50 mV dec^{-1}, which is noticeably lower than those of NiFeP (112 mV dec^{-1}), CoFeP (102 mV dec^{-1}), and NiCoP (88 mV dec^{-1}). This result strongly suggests that the $NiCoFe_xP$ produces hydrogen via a combined Volmer−Heyrovsky mechanism.[70] Another rational measurement of double-layer capacitances (C_{dl}) is herein employed, which is directly related to the electrochemical surface area (ECSA).[71] Derived from cyclic voltammograms (CVs) vs the scan rate in 1.0 M KOH (Figure S4), the C_{dl} of 32.62 mF cm^{-2} on $NiCoFe_xP/CC$ is much higher than that on NiFeP/CC (14.36 mF cm^{-2}), CoFeP/CC (19.56 mF cm^{-2}),

DOI: 10.1021/acssuschemeng.7b04808
ACS Sustainable Chem. Eng. 2018, 6, 6146−6156

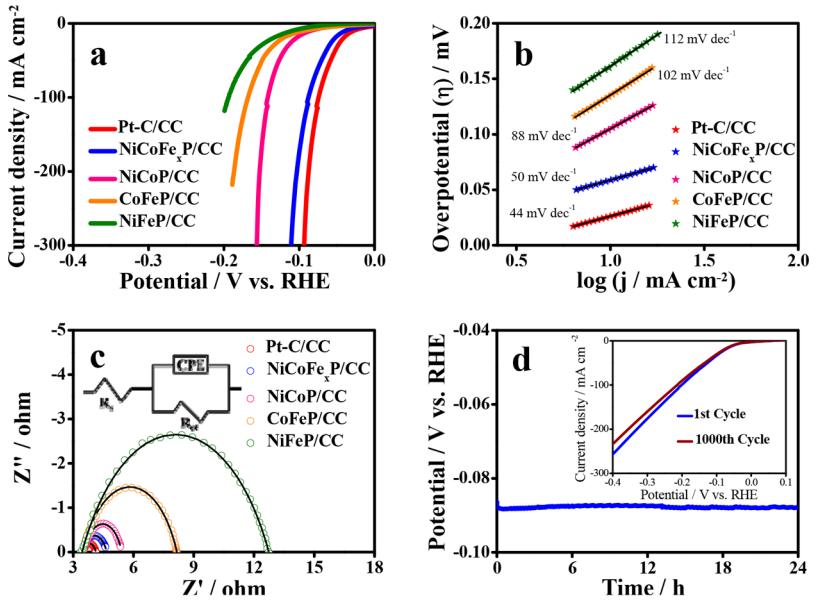

Figure 4. (a) *iR*-corrected polarization curve of $NiCoFe_xP/CC$ for HER in 1.0 M KOH solution at 2 mV s^{-1} scan rate. The corresponding curves of Pt−C, NiCoP, CoFeP, and NiFeP/CC are presented for comparison. (b) Polarization curve-derived Tafel plots of the electrocatalysts. (c) Nyquist plots of the catalysts at −0.2 V vs RHE. (d) Long-term stability study by using chronopotentiometric technique at 100 mA cm^{-2} current density. Inset indicates durability of $NiCoFe_xP/CC$ after 1000 CV cycles.

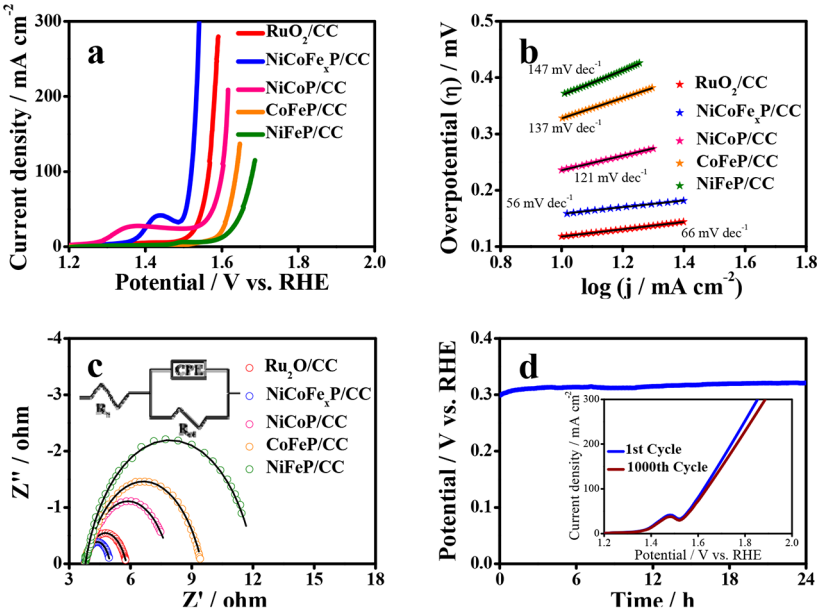

Figure 5. (a) *iR*-corrected polarization curve for OER in 1.0 M KOH solution at 2 mV s^{-1} scan rate. (b) Corresponding Tafel plots. (c) EIS graphs at 1.56 V vs RHE of all the synthesized catalysts. (d) Chronopotentiometric analysis at a constant 100 mA cm^{-2} current density. Inset represents durability investigation of $NiCoFe_xP/CC$ after 1000 CV cycles.

and NiCoP/CC (22.49 mF cm^{-2}). The higher C_{dl} value implies the enriched active sites on $NiCoFe_xP/CC$. Meanwhile, EIS displays the varied charge-transfer resistance in as-prepared electrocatalysts (Figure 4c). Likewise, the sequence of HER performance is that $NiCoFe_xP/CC$ delivers an R_{ct} value obviously lower than those of NiFeP, CoFeP, and NiCoP/CC (Table S2). This suggests rapid electron transport for H_2 evolution on the 2D $NiCoFe_xP$ nanoplates directly grown on CC. To access the electrochemical HER stability of $NiCoFe_xP$, a long-term HER was conducted at 100 mA cm^{-2} in alkaline electrolyte. Figure 4d demonstrates that the $NiCoFe_xP$ retains 92.7% of its original HER activity, after 24 h of H_2 release even at high current density. Inset of the Figure 4d represents high durability of $NiCoFe_xP/CC$ toward HER after 1000 cyclic voltammetry cycles.

$NiCoFe_xP/CC$ was further explored with respect to the electrocatalytic OER in alkaline medium (1.0 M KOH). Figure 5a displays the *iR*-corrected LSV plots of $NiCoFe_xP$, NiFeP, CoFeP, and NiCoP at 2 mV s^{-1} scan rates, along with that of the benchmark RuO_2/CC with the same mass loading. NiFeP, CoFeP, and NiCoP present η_{50} values (at 50 mA cm^{-2}) of 425, 389, and 346 mV, respectively. By contrast, $NiCoFe_xP$ shows remarkably improved activity with a low η_{50} and η_{100} of 275 and 290 mV, outperforming the conventional RuO_2 on CC (η_{50} =

DOI: 10.1021/acssuschemeng.7b04808
ACS Sustainable Chem. Eng. 2018, 6, 6146−6156

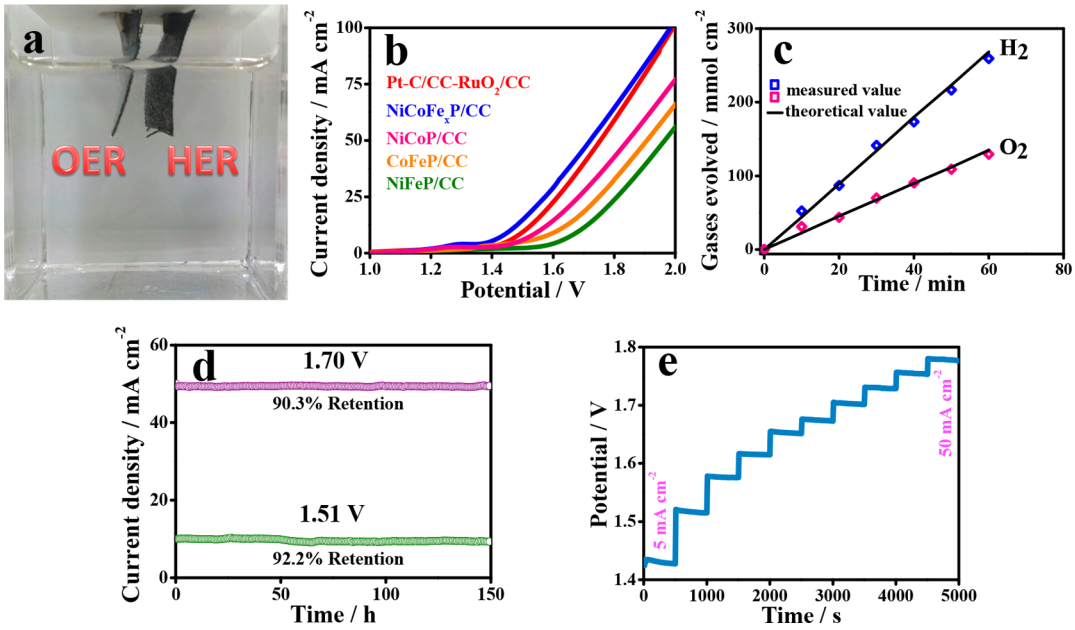

Figure 6. (a) Digital image of water splitting by NiCoFe$_x$P/CC. (b) Polarization curves for NiCoFe$_x$P/CC, Pt−C/CC−RuO$_2$/CC, and other catalysts in a two-electrode system under 1.0 M KOH electrolyte without *iR*-correction. (c) Faraday efficiencies of H_2 and O_2 production by NiCoFe$_x$P/CC. (d) Chronoamperometric curves for water electrolysis by NiCoFe$_x$P/CC at different potentials. (e) Multicurrent process for NiCoFe$_x$P/CC.

318 mV and η_{100} = 335 mV). The Tafel slopes for NiCoFe$_x$P, NiCoP, CoFeP, and NiFeP are around 56, 121, 137, and 147 mV dec^{-1}, respectively (Figure 5b). The low Tafel slope value strongly suggests that NiCoFe$_x$P activates water oxidation kinetics. Coincident with the OER activity, NiCoFe$_x$P exhibits an R_{ct} smaller than those of NiFeP, CoFeP, and NiCoP (Figure 5c), indicating the fast Faradaic process on the NiCoFe$_x$P nanohybrids. NiCoFe$_x$P retained steady OER activity with >90% retention of initial potential even after 24 h chronopotentiometric analysis at 100 mA cm^{-2} (Figure 5d). The high durable OER activity is confirmed from the inset of Figure 5d. Thus, in heterogeneous catalysts, existence of a higher number of metals facilitates the occurrence of multiple valence cations with more complicated electronic structures and higher conductivity. This characteristic helps to pull down the thermodynamic energy barrier of proton-coupled electron pre-equilibrium by assisting O−O bond formation; therefore, the improved catalytic activity is achieved.

Moreover, the ECSA normalized HER and OER profiles (Figure S5) also favor the NiCoFe$_x$P/CC, concluding it is intrinsically more active compared to other as-synthesized catalysts.

Because of excellent electrocatalytic performance for NiCoFe$_x$P/CC toward HER and OER in alkaline solutions, NiCoFe$_x$P/CC was used as anode and cathode together toward full water splitting in 1.0 M KOH. Figure 6a represents the digital photo of the two-electrode system which clearly shows evolution of gases from both the electrodes. A current density of 10 mA cm^{-2} was delivered by NiCoFe$_x$P/CC nanohybrids at around 1.51 V. Figure 6b reveals that the overall water splitting activity of NiCoFe$_x$P is much higher than those of Pt−C/CC−RuO$_2$/CC couple (1.54 V) and the NiFeP (1.687 V), CoFeP (1.618 V), and NiCoP (1.586 V) electrodes, indicating its compatible integration of HER and OER activities associated with its hierarchical structures and successful surface functionalization. The overpotential value for NiCoFe$_x$P/CC is lower than those of recently reported various nonprecious metal-based overall splitting electrocatalysts (Table S2). In addition, the Faradaic efficiencies for H_2 and O_2 evolution were calculated by comparing the experimentally measured gas quantity with the theoretically evaluated gas amount.[72] The resemblance of both values (Figure 6c) indicates efficiencies of ∼100% for both HER and OER, which eliminates O_2 reduction at the cathode and H_2 oxidation at the anode. Moreover, the electrodes show negligible degradation in stability with current densities of ∼10 and 50 mA cm^{-2} for 150 h when the applied voltage is set to 1.51 and 1.70 V, respectively, confirming the satisfactory long-term durability of NiCoFe$_x$P/CC in the strongly alkaline electrolyte (Figure 6d). Figure 6e shows the results of a multistep chronopotentiometric analysis of NiCoFe$_x$P electrode in 1.0 M KOH. Precisely, a staircase current density was applied from 5 to 50 mA cm^{-2} with increments of 5 mA cm^{-2} per 500 s. Initially with application of different amount current density a sudden increase in potential value is observed, but afterward it remains constant for the residual 500 s, specifically at high current. This fast chronopotentiometric response suggests exceptionally high mass transport behavior (i.e., diffusion of water molecules toward inward direction and dissipation of O_2 bubbles in reverse track) and high conductivity of the NiCoFe$_x$P electrode.[73]

TEM analysis was carried out after catalysis (Figures S6a and b). In both cases the material loses its crystallinity, becomes aggregated, and their individual presence, i.e., separate nanoparticles could not be observed, suggesting strong interactions between the nanocomponents. To elucidate HER and OER mechanisms on NiCoFe$_x$P/CC, the catalysts were subjected to XPS analysis after HER and OER were performed (Figures S6c−f). As shown in XPS spectra of Co 2p, Ni 2p, and Fe 2p, the peak corresponding to metal−P bond completely vanished after OER. The peaks after the OER can be assigned to oxidized metal states only. For P 2p, the total P signal

DOI: 10.1021/acssuschemeng.7b04808
ACS Sustainable Chem. Eng. 2018, 6, 6146−6156

Table 1. Comparison of Representative Transition-Metal-Based Water-Splitting Catalysts in Alkaline Electrolyte

catalysts	overpotential for HER (mV)	overpotential for OER (mV)	cell voltage for overall water splitting (V)	references
NiCoP/CC	η_{10} = 62	η_{10} = 242	η_{10} = 1.524	ref 14
$NiMoP_2$ NW/CC	η_{100} = 199	η_{100} = 330	η_{10} = 1.67	ref 20
NiCoP/NF	η_{10} = 32	η_{50} = 280	η_{10} = 1.58	ref 53
NiCoFe LTHs/CFC	η_{10} = 200	η_{10} = 239	η_{10} = 1.55	ref 54
NiCoP NWAs	η_{10} = 104	η_{100} = 370	η_{20} = 1.64	ref 77
$Ni_{1.5}Fe_{0.5}P$/CF	η_{10} = 282	η_{10} = 264	η_{10} = 1.589	ref 81
NiCoP/Ni foam	η_{50} = 133	η_{50} = 308	η_{50} = 1.77	ref 82
NiCoP/rGO	η_{10} = 209	η_{10} = 270	η_{10} = 1.59	ref 83
$Ni_{0.51}Co_{0.49}P$ film	η_{10} = 82	η_{10} = 239	η_{10} = 1.57	ref 84
NiCuP	η_{50} = 146	η_{10} = 292	η_{20} = 1.6	ref 85
Co4Ni1P NTs	η_{10} = 129	η_{10} = 245	η_{10} = 1.59	ref 86
$Ni_{2.5}Co_{0.5}Fe$ LDH/NF	η_{40} = 200	η_{40} = 310	η_{10} = 1.62	ref 87
MoP/Ni_2P/NF	η_{10} = 75	η_{20} = 309	η_{10} = 1.55	ref 88
$NiCoFe_xP$/CC	**η_{10} = 39**	**η_{50} = 275**	**η_{10} = 1.51**	**this work**

intensity also dramatically decreases, and only the broad hump at 133.9 eV for oxidized phosphorus components is observed. These results indicate the surface oxidation of $NiCoFe_xP$ and P is being leached out from catalyst surface to electrolyte as phosphate over time, whereas the metal leach out rate is much lower. Furthermore, these conversions are ineffective regarding stability of the electrode. As water oxidation catalysis is assisted by surface phosphate via proton coupled electron transfer, the decrease in activity over time may be ascribed to the surface-bound phosphate ion loss.[74−76] Therefore, the high OER activity of $NiCoFe_xP$ originates from the formation of Ni−Co−Fe phosphate species on the catalyst surface during OER in the strong alkaline medium.[14] Common transition-metal phosphates and also the amorphous phosphate layer are proficient electrocatalysts toward full water splitting in alkaline electrolyte. The alkaline medium electrolysis facilitates formation of catalytically active Ni−Co−Fe-phosphate layer on the surface of $NiCoFe_xP$. In situ generated Ni−Co−Fe−phosphate/$NiCoFe_xP$ heterojunction is the most important factor of significantly high stability of the catalytic system in the OER. The Raman spectra of the $NiCoFe_xP$ before and after OER also confirm the surface oxidation and formation of nickel and cobalt oxyhydroxides on the catalyst surface after OER process (Figure S7).

Generally, the OER process includes four consecutive stages:[77,78]

$$M_{cat} + OH^-(aq) \rightarrow M_{cat}OH_{ads} + e^- \quad (1)$$

$$OH^-(aq) + M_{cat}OH_{ads} \rightarrow H_2O(l) + e^- + M_{cat}O_{ads} \quad (2)$$

$$M_{cat}O_{ads} + OH^-(aq) \rightarrow M_{cat}OOH_{ads} + e^- \quad (3)$$

$$2M_{cat}O_{ads} \rightarrow O_2(g) \quad (4)$$

$$M_{cat}OOH_{ads} + OH^-(aq) \rightarrow M_{cat} + O_2(g) + H_2O(l) \quad (5)$$

The probable mechanism of OER to phosphate catalysts is, in the first stage, H_2O is adsorbed on the active site of the catalyst, and dissociation of water molecule generates $M_{cat}OH_{ads}$ species. In second step, loss of another proton provides $M_{cat}O_{ads}$. The coupling between adsorbed oxygen atom (O_{ads}) and H_2O leads to formation of $M_{cat}OOH_{ad}$. At last, recombination of O_{ads} species and dissociation of the proton from $M_{cat}OOH_{ads}$ originates in oxygen evolution. However, the changes in the oxidation state of metals is an indispensable part of the OER mechanism.

Following long-term stability, the XPS spectrum of Co 2p in post-HER sample showed the fading of cobalt phosphide's peak from its original position (Figure S6c). XPS spectrum of Ni 2p (Figure S6d) also describes presence of oxidized Ni in the surface layer instead of nickel phosphide. Again, Fe 2p XPS spectrum (Figure S6e) indicates the dominating peak ascribed as Fe^{3+}. Moreover, a slight shift to the binding energy value of P−O species (133.9 eV) is observed in the XPS spectrum of P 2p, and the peak near 129.8 eV almost vanished (Figure S6f). These changes in XPS spectra of different elements suggest the appearance of a new layer of oxide phases (perhaps Ni−Co−Fe phosphate and/or partially oxidized Ni−Co−Fe oxide/hydroxide). The synergistic interaction between metal phosphide and in situ originated oxidized metal−phosphate layer or newly formed amorphous partially metal oxides/hydroxides layer helps to achieve excellent HER activity and superb stability.

The Tafel slope of $NiCoFe_xP$/CC suggests that the HER proceeds via the Tafel−Volmer−Heyrovsky mechanisms:[77,79]

$$M_{cat} + H_2O(l) + e^- \rightarrow M_{cat}H_{ads} + OH^-(aq)\ (Volmer) \quad (6)$$

$$2M_{cat}H_{ads} \rightarrow 2M_{cat} + H_2(g)\ (Tafel) \quad (7)$$

$$M_{cat}H_{ads} + H_2O(l) + e^- \rightarrow M_{cat} + H_2(g) + OH^-(aq)\ (Heyrovsky) \quad (8)$$

As-synthesized $NiCoFe_xP$/CC has a structure similar to that of Ni−Fe-based hydrogenase enzyme. Further, the mechanism of HER by $NiCoFe_xP$/CC is similar to the HER activity of Ni−Fe-based hydrogenase (for detailed discussion, see HER mechanism section in Supporting Information).

Therefore, on the basis of all discussions, the HER mechanism for $NiCoFe_xP$ in alkaline medium can be described in three steps. (1) The electrical double layer formed by water molecule on the catalyst surface helps to weaken the H−OH bond by electronic effects. In general, when a water molecule is adsorbed on the surface of $NiCoFe_xP$, the H−OH bond will be weakened by the interaction between the under-coordinated metal center ($M^{\delta+}$, M = Ni, Co, Fe) and the O atom as well as the interaction between the dangling P atom ($P^{\delta-}$) and H atom.[80] (2) The dissociation of water molecule into H^+ and OH^- occurs with the help of free electrons. (3) The H atoms

DOI: 10.1021/acssuschemeng.7b04808
ACS Sustainable Chem. Eng. 2018, 6, 6146−6156

aretransferred to vacant metal sites, next to which are covered by OH^- from the phosphide center. Then, H atoms adsorbed on metal site are denoted as H_{ads}. Therefore, the whole HER process is completed after H_{ads} recombination and OH^- desorption. The high electron localization on P atom in metal phosphides facilitates the adsorption of H^+ ions and dissociation of water molecules.

Because of OH^- species, the catalyst surface becomes slightly oxidized. Thus, the above discussion demonstrates the continuous development of new catalyst layer on the $NiCoFe_xP$ surface (evidently NiCoFe−phosphate layer). The successive performance of the achieved catalytic system ensures superior catalytic activity, accredited to the pre-existing phosphide nanoplates, which guarantee appropriate charge transfer between the newly formed catalyst layer and the CC substrate. It is important to note that our developed material $NiCoFe_xP$/CC outperforms many leading nonprecious-metal-based catalysts for HER and OER, and also full water splitting in an alkaline medium as demonstrated in Table 1.[14,20,53,54,77,81−88]

Further, to assess the intrinsic electrochemical property of the as-synthesized $NiCoFe_xP$/CC the HER, OER and two-electrode full water splitting activities were also investigated in acidic (0.5 M H_2SO_4, pH 1.0) and neutral (1.0 M PBS, pH 7.0) electrolyte (Figure S8). These results demonstrate the good water splitting activity with excellent stability of the $NiCoFe_xP$/CC electrocatalyst under all pH conditions.

To understand the effect of Fe-doping in nickel and cobalt phosphide, we synthesized bare nickel phosphide (NiP) and cobalt phosphide (CoP) on CC using the same reaction protocol. The HER, OER, and two-electrode full water splitting performances of NiP and CoP/CC with nearly same loading amount is also measured under 1.0 M KOH electrolyte. Figure S9 clearly indicates the lower catalytic activity of NiP and CoP/CC compared to that of other Fe-doped electrocatalysts. Thus, incorporation of Fe-ions in catalyst helps to enhance conductivity through a synergistic effect between metal ions, and as a result, electrocatalysts possess inherently high catalytic activity.

To further investigate the role of the ratio of cation centers in hybrid material toward electrochemical HER and OER, the nanostructures with different molar contents of Fe(III) were synthesized on carbon cloth (Figure S10). By using different Ni:Co:Fe molar ratios (1:1:0.1, 1:1:0.2, 1:1:0.5, and 1:1:1) in the precursors, a series of ternary metal phosphides were synthesized on CC by the same reaction protocol, and Table S1 represents the actual product Ni:Co:Fe molar ratio determined by ICP-OES. The XRD patterns of the different catalysts with different Fe(III) contents are quite similar to that of NiCoP, as shown in Figure S10a. The peaks for $NiCoFe_xP$ are slightly shifted to larger 2θ values compared to those of NiCoP because of Fe(III) component incorporation. The effect of Ni:Co:Fe molar ratio on the morphology was also studied. Figures S10b−d show FESEM images of $NiCoFe_{0.1}P$, $NiCoFe_{0.2}P$, $NiCoFe_{0.5}P$, and $NiCoFe_{1.0}P$, respectively. It can be clearly seen that a lower Fe content tends to produce a nanoarray, while a higher Fe content produces nanoplate morphology. Then, the HER and OER activities of different composites were investigated (Table S3). Figure S11a shows that the $NiCoFe_{0.1}P$, $NiCoFe_{0.2}P$, $NiCoFe_{0.5}P$, and $NiCoFe_{1.0}P$/CC required overpotentials of 310, 270, 52, and 145 mV at 10 mA cm^{-2} for HER, respectively. Similarly, in the case of OER, the $NiCoFe_{0.1}P$, $NiCoFe_{0.2}P$, $NiCoFe_{0.5}P$, and $NiCoFe_{1.0}P$/CC provide 510, 410, 320, and 370 mV overpotentials, respectively at 50 mA cm^{-2} current density (Figure S11d). Thus, the Fe(III) content plays a crucial role in modulating electronic structure, which is responsible for the enhanced electrochemical hydrogen and oxygen evolution. Moreover, in the both the HER and OER, $NiCoFe_{0.5}P$ shows a very low R_{ct} value compared to those of the other composites (Figures S11b and e). This result also indicates higher catalytic activity owing to superior electron transport. Chronoamperometry was used to investigate the stability of the composites in the HER and OER. Figures S11c and f clearly show that with an increase in Fe(III) content from $NiCoFe_{0.1}P$ to $NiCoFe_{0.2}P$, the stability of the catalyst slightly increases. Further Fe(III) increase ($NiCoFe_{0.5}P$) enhances the stability dramatically. For both the HER and OER, $NiCoFe_{0.5}P$/CC shows >90% stability upon prolonged (24 h) use. However, with a further increase in Fe(III) content from 0.5 to 1 mmol, the stability decreases. Figure S12 also confirms the higher activity of $NiCoFe_{0.5}P$ compared to others by possessing higher C_{dl} value as well as ECSA (Table S3). These results confirm that the 2D nanoplate-like structure of $NiCoFe_{0.5}P$/CC provides a faster charge transfer rate and facile release of the evolved H_2 for improved HER and OER activity as well as excellent stability.

CONCLUSIONS

A new trimetallic phosphide electrocatalyst grown on CC with impressive catalytic activity toward overall water splitting is presented. Direct growth of nanoplates onto CC with equal distribution of all elements, rapid charge transfer capability imparted by open spaces between the nanoplates, and the self-standing feature of $NiCoFe_xP$/CC are collectively responsible for its excellent activity and stability in the HER and OER. Moreover, the synergistic effect of the different metal centers contributes to the impressive overall water splitting performance. This study demonstrates a new range of ternary transition-metal-based phosphides (TMPs) as high-performance electrocatalysts for overall water splitting.

ASSOCIATED CONTENT

Supporting Information

The Supporting Information is available free of charge on the ACS Publications website at DOI: 10.1021/acssuschemeng.7b04808.

Figures of electrocatalytic activity, FESEM images, elemental area mapping, XPS spectra, electrochemical data, and TEM images; tables for comparison of HER and OER activity (PDF)

AUTHOR INFORMATION

Corresponding Author

*E-mail: scj@yonsei.ac.kr; Fax: +82-2-312-2159; Tel: +82-2-2123-5817.

ORCID

Chaiti Ray: 0000-0003-1260-156X
Bingjun Jin: 0000-0002-6444-583X
Aniruddha Kundu: 0000-0002-6508-6728
Jong Hyeok Park: 0000-0002-6629-3147
Seong Chan Jun: 0000-0001-6986-8308

Notes

The authors declare no competing financial interest.

DOI: 10.1021/acssuschemeng.7b04808
ACS Sustainable Chem. Eng. 2018, 6, 6146−6156

■ ACKNOWLEDGMENTS

This research was supported by Nano-Material Technology Development Program (NRF-2017M3A7B4041987) through the National Research Foundation of Korea (NRF).

■ REFERENCES

(1) Mazloomi, K.; Gomes, C. Hydrogen as an energy carrier: Prospects and challenges. *Renewable Sustainable Energy Rev.* **2012**, *16* (5), 3024−3033.
(2) Ray, C.; Dutta, S.; Negishi, Y.; Pal, T. A new stable Pd-Mn3O4 nanocomposite as an efficient electrocatalyst for the hydrogen evolution reaction. *Chem. Commun.* **2016**, *52* (36), 6095−6098.
(3) Anantharaj, S.; Karthick, K.; Venkatesh, M.; Simha, T. V. S. V.; Salunke, A. S.; Ma, L.; Liang, H.; Kundu, S. Enhancing electrocatalytic total water splitting at few layer Pt-NiFe layered double hydroxide interfaces. *Nano Energy* **2017**, *39*, 30−43.
(4) Duan, H.; Li, D.; Tang, Y.; He, Y.; Ji, S.; Wang, R.; Lv, H.; Lopes, P. P.; Paulikas, A. P.; Li, H.; Mao, S. X.; Wang, C.; Markovic, N. M.; Li, J.; Stamenkovic, V. R.; Li, Y. High-Performance Rh2P Electrocatalyst for Efficient Water Splitting. *J. Am. Chem. Soc.* **2017**, *139* (15), 5494−5502.
(5) Jiao, Y.; Zheng, Y.; Jaroniec, M.; Qiao, S. Z. Design of electrocatalysts for oxygen- and hydrogen-involving energy conversion reactions. *Chem. Soc. Rev.* **2015**, *44* (8), 2060−2086.
(6) Ahn, S. H.; Manthiram, A. Direct growth of ternary Ni-Fe-P porous nanorods onto nickel foam as a highly active, robust bifunctional electrocatalyst for overall water splitting. *J. Mater. Chem. A* **2017**, *5* (6), 2496−2503.
(7) Tang, C.; Zhang, R.; Lu, W.; Wang, Z.; Liu, D.; Hao, S.; Du, G.; Asiri, A. M.; Sun, X. Energy-Saving Electrolytic Hydrogen Generation: Ni2P Nanoarray as a High-Performance Non-Noble-Metal Electrocatalyst. *Angew. Chem., Int. Ed.* **2017**, *56* (3), 842−846.
(8) Zhu, Y.; Zhou, W.; Zhong, Y.; Bu, Y.; Chen, X.; Zhong, Q.; Liu, M.; Shao, Z. A Perovskite Nanorod as Bifunctional Electrocatalyst for Overall Water Splitting. *Adv. Energy Mater.* **2017**, *7* (8), 1602122.
(9) Zhang, J.; Wang, T.; Pohl, D.; Rellinghaus, B.; Dong, R.; Liu, S.; Zhuang, X.; Feng, X. Interface Engineering of MoS2/Ni3S2 Heterostructures for Highly Enhanced Electrochemical Overall-Water-Splitting Activity. *Angew. Chem., Int. Ed.* **2016**, *55* (23), 6702−6707.
(10) Jia, Y.; Zhang, L.; Gao, G.; Chen, H.; Wang, B.; Zhou, J.; Soo, M. T.; Hong, M.; Yan, X.; Qian, G.; Zou, J.; Du, A.; Yao, X. A Heterostructure Coupling of Exfoliated Ni−Fe Hydroxide Nanosheet and Defective Graphene as a Bifunctional Electrocatalyst for Overall Water Splitting. *Adv. Mater.* **2017**, *29* (17), 1700017.
(11) Wang, J.; Cui, W.; Liu, Q.; Xing, Z.; Asiri, A. M.; Sun, X. Recent Progress in Cobalt-Based Heterogeneous Catalysts for Electrochemical Water Splitting. *Adv. Mater.* **2016**, *28* (2), 215−230.
(12) Jin, Y.; Yue, X.; Shu, C.; Huang, S.; Shen, P. K. Three-dimensional porous MoNi4 networks constructed by nanosheets as bifunctional electrocatalysts for overall water splitting. *J. Mater. Chem. A* **2017**, *5* (6), 2508−2513.
(13) Tang, C.; Gan, L.; Zhang, R.; Lu, W.; Jiang, X.; Asiri, A. M.; Sun, X.; Wang, J.; Chen, L. Ternary FexCo1−xP Nanowire Array as a Robust Hydrogen Evolution Reaction Electrocatalyst with Pt-like Activity: Experimental and Theoretical Insight. *Nano Lett.* **2016**, *16* (10), 6617−6621.
(14) Du, C.; Yang, L.; Yang, F.; Cheng, G.; Luo, W. Nest-like NiCoP for Highly Efficient Overall Water Splitting. *ACS Catal.* **2017**, *7* (6), 4131−4137.
(15) Li, W.; Gao, X.; Xiong, D.; Wei, F.; Song, W.-G.; Xu, J.; Liu, L. Hydrothermal Synthesis of Monolithic Co3Se4 Nanowire Electrodes for Oxygen Evolution and Overall Water Splitting with High Efficiency and Extraordinary Catalytic Stability. *Adv. Energy Mater.* **2017**, *7* (17), 1602579.
(16) Dutta, S.; Ray, C.; Negishi, Y.; Pal, T. Facile Synthesis of Unique Hexagonal Nanoplates of Zn/Co Hydroxy Sulfate for Efficient Electrocatalytic Oxygen Evolution Reaction. *ACS Appl. Mater. Interfaces* **2017**, *9* (9), 8134−8141.
(17) Tian, L.; Yan, X.; Chen, X. Electrochemical Activity of Iron Phosphide Nanoparticles in Hydrogen Evolution Reaction. *ACS Catal.* **2016**, *6* (8), 5441−5448.
(18) Yu, L.; Yang, J. F.; Guan, B. Y.; Lu, Y.; Lou, X. W. Hierarchical Hollow Nanoprisms Based on Ultrathin Ni-Fe Layered Double Hydroxide Nanosheets with Enhanced Electrocatalytic Activity towards Oxygen Evolution. *Angew. Chem.* **2018**, *130* (1), 178−182.
(19) Guan, B. Y.; Yu, L.; Lou, X. W. General Synthesis of Multishell Mixed-Metal Oxyphosphide Particles with Enhanced Electrocatalytic Activity in the Oxygen Evolution Reaction. *Angew. Chem., Int. Ed.* **2017**, *56* (9), 2386−2389.
(20) Wang, X.-D.; Chen, H.-Y.; Xu, Y.-F.; Liao, J.-F.; Chen, B.-X.; Rao, H.-S.; Kuang, D.-B.; Su, C.-Y. Self-supported NiMoP2 nanowires on carbon cloth as an efficient and durable electrocatalyst for overall water splitting. *J. Mater. Chem. A* **2017**, *5* (15), 7191−7199.
(21) Wang, X.; Li, W.; Xiong, D.; Liu, L. Fast fabrication of self-supported porous nickel phosphide foam for efficient, durable oxygen evolution and overall water splitting. *J. Mater. Chem. A* **2016**, *4* (15), 5639−5646.
(22) Song, J.; Zhu, C.; Xu, B. Z.; Fu, S.; Engelhard, M. H.; Ye, R.; Du, D.; Beckman, S. P.; Lin, Y. Bimetallic Cobalt-Based Phosphide Zeolitic Imidazolate Framework: CoP_x Phase-Dependent Electrical Conductivity and Hydrogen Atom Adsorption Energy for Efficient Overall Water Splitting. *Adv. Energy Mater.* **2017**, *7* (2), 1601555.
(23) Pan, Y.; Hu, W.; Liu, D.; Liu, Y.; Liu, C. Carbon nanotubes decorated with nickel phosphide nanoparticles as efficient nanohybrid electrocatalysts for the hydrogen evolution reaction. *J. Mater. Chem. A* **2015**, *3* (24), 13087−13094.
(24) Pan, Y.; Chen, Y.; Lin, Y.; Cui, P.; Sun, K.; Liu, Y.; Liu, C. Cobalt nickel phosphide nanoparticles decorated carbon nanotubes as advanced hybrid catalysts for hydrogen evolution. *J. Mater. Chem. A* **2016**, *4* (38), 14675−14686.
(25) Pan, Y.; Liu, Y.; Lin, Y.; Liu, C. Metal Doping Effect of the M−Co2P/Nitrogen-Doped Carbon Nanotubes (M = Fe, Ni, Cu) Hydrogen Evolution Hybrid Catalysts. *ACS Appl. Mater. Interfaces* **2016**, *8* (22), 13890−13901.
(26) Pan, Y.; Lin, Y.; Chen, Y.; Liu, Y.; Liu, C. Cobalt phosphide-based electrocatalysts: synthesis and phase catalytic activity comparison for hydrogen evolution. *J. Mater. Chem. A* **2016**, *4* (13), 4745−4754.
(27) Pan, Y.; Lin, Y.; Liu, Y.; Liu, C. A novel CoP/MoS2-CNTs hybrid catalyst with Pt-like activity for hydrogen evolution. *Catal. Sci. Technol.* **2016**, *6* (6), 1611−1615.
(28) Feng, L.-L.; Yu, G.; Wu, Y.; Li, G.-D.; Li, H.; Sun, Y.; Asefa, T.; Chen, W.; Zou, X. High-Index Faceted Ni3S2 Nanosheet Arrays as Highly Active and Ultrastable Electrocatalysts for Water Splitting. *J. Am. Chem. Soc.* **2015**, *137* (44), 14023−14026.
(29) Chen, P.; Zhou, T.; Zhang, M.; Tong, Y.; Zhong, C.; Zhang, N.; Zhang, L.; Wu, C.; Xie, Y. 3D Nitrogen-Anion-Decorated Nickel Sulfides for Highly Efficient Overall Water Splitting. *Adv. Mater.* **2017**, *29* (30), 1701584.
(30) Kwak, I. H.; Im, H. S.; Jang, D. M.; Kim, Y. W.; Park, K.; Lim, Y. R.; Cha, E. H.; Park, J. CoSe2 and NiSe2 Nanocrystals as Superior Bifunctional Catalysts for Electrochemical and Photoelectrochemical Water Splitting. *ACS Appl. Mater. Interfaces* **2016**, *8* (8), 5327−5334.
(31) Yu, B.; Wang, X.; Qi, F.; Zheng, B.; He, J.; Lin, J.; Zhang, W.; Li, Y.; Chen, Y. Self-Assembled Coral-like Hierarchical Architecture Constructed by $NiSe_2$ Nanocrystals with Comparable Hydrogen-Evolution Performance of Precious Platinum Catalyst. *ACS Appl. Mater. Interfaces* **2017**, *9* (8), 7154−7159.
(32) Gong, M.; Zhou, W.; Tsai, M.-C.; Zhou, J.; Guan, M.; Lin, M.-C.; Zhang, B.; Hu, Y.; Wang, D.-Y.; Yang, J.; Pennycook, S. J.; Hwang, B.-J.; Dai, H. Nanoscale nickel oxide/nickel heterostructures for active hydrogen evolution electrocatalysis. *Nat. Commun.* **2014**, *5*, 4695.
(33) Rao, Y.; Wang, Y.; Ning, H.; Li, P.; Wu, M. Hydrotalcite-like $Ni(OH)_2$ Nanosheets in Situ Grown on Nickel Foam for Overall

DOI: 10.1021/acssuschemeng.7b04808
ACS Sustainable Chem. Eng. 2018, 6, 6146−6156

Water Splitting. *ACS Appl. Mater. Interfaces* **2016**, *8* (49), 33601−33607.
(34) Los, P.; Lasia, A. Electrocatalytic properties of amorphous nickel boride electrodes for hydrogen evolution reaction in alkaline solution. *J. Electroanal. Chem.* **1992**, *333* (1), 115−125.
(35) Popczun, E. J.; McKone, J. R.; Read, C. G.; Biacchi, A. J.; Wiltrout, A. M.; Lewis, N. S.; Schaak, R. E. Nanostructured Nickel Phosphide as an Electrocatalyst for the Hydrogen Evolution Reaction. *J. Am. Chem. Soc.* **2013**, *135* (25), 9267−9270.
(36) Sun, Y.; Hang, L.; Shen, Q.; Zhang, T.; Li, H.; Zhang, X.; Lyu, X.; Li, Y. Mo doped Ni2P nanowire arrays: an efficient electrocatalyst for the hydrogen evolution reaction with enhanced activity at all pH values. *Nanoscale* **2017**, *9*, 16674.
(37) Ledendecker, M.; Krick Calderón, S.; Papp, C.; Steinrück, H.-P.; Antonietti, M.; Shalom, M. The Synthesis of Nanostructured Ni5P4 Films and their Use as a Non-Noble Bifunctional Electrocatalyst for Full Water Splitting. *Angew. Chem., Int. Ed.* **2015**, *54* (42), 12361−12365.
(38) Xu, J.; Wei, X.-K.; Costa, J. D.; Lado, J. L.; Owens-Baird, B.; Gonçalves, L. P. L.; Fernandes, S. P. S.; Heggen, M.; Petrovykh, D. Y.; Dunin-Borkowski, R. E.; Kovnir, K.; Kolen'ko, Y. V. Interface Engineering in Nanostructured Nickel Phosphide Catalyst for Efficient and Stable Water Oxidation. *ACS Catal.* **2017**, *7* (8), 5450−5455.
(39) Wang, M.; Lin, M.; Li, J.; Huang, L.; Zhuang, Z.; Lin, C.; Zhou, L.; Mai, L. Metal-organic framework derived carbon-confined Ni2P nanocrystals supported on graphene for an efficient oxygen evolution reaction. *Chem. Commun.* **2017**, *53* (59), 8372−8375.
(40) Kibsgaard, J.; Tsai, C.; Chan, K.; Benck, J. D.; Norskov, J. K.; Abild-Pedersen, F.; Jaramillo, T. F. Designing an improved transition metal phosphide catalyst for hydrogen evolution using experimental and theoretical trends. *Energy Environ. Sci.* **2015**, *8* (10), 3022−3029.
(41) Yu, J.; Cheng, G.; Luo, W. Hierarchical NiFeP microflowers directly grown on Ni foam for efficient electrocatalytic oxygen evolution. *J. Mater. Chem. A* **2017**, *5* (22), 11229−11235.
(42) Mendoza-Garcia, A.; Su, D.; Sun, S. Sea urchin-like cobalt-iron phosphide as an active catalyst for oxygen evolution reaction. *Nanoscale* **2016**, *8* (6), 3244−3247.
(43) He, P.; Yu, X.-Y.; Lou, X. W. Carbon-Incorporated Nickel−Cobalt Mixed Metal Phosphide Nanoboxes with Enhanced Electrocatalytic Activity for Oxygen Evolution. *Angew. Chem.* **2017**, *129* (14), 3955−3958.
(44) Feng, Y.; Yu, X.-Y.; Paik, U. Nickel cobalt phosphides quasi-hollow nanocubes as an efficient electrocatalyst for hydrogen evolution in alkaline solution. *Chem. Commun.* **2016**, *52* (8), 1633−1636.
(45) Li, Y.; Liu, J.; Chen, C.; Zhang, X.; Chen, J. Preparation of NiCoP Hollow Quasi-Polyhedra and Their Electrocatalytic Properties for Hydrogen Evolution in Alkaline Solution. *ACS Appl. Mater. Interfaces* **2017**, *9* (7), 5982−5991.
(46) Yang, N.; Tang, C.; Wang, K.; Du, G.; Asiri, A. M.; Sun, X. Iron-doped nickel disulfide nanoarray: A highly efficient and stable electrocatalyst for water splitting. *Nano Res.* **2016**, *9* (11), 3346−3354.
(47) Wang, Y.; Xie, C.; Liu, D.; Huang, X.; Huo, J.; Wang, S. Nanoparticle-Stacked Porous Nickel−Iron Nitride Nanosheet: A Highly Efficient Bifunctional Electrocatalyst for Overall Water Splitting. *ACS Appl. Mater. Interfaces* **2016**, *8* (29), 18652−18657.
(48) Wang, P.; Pu, Z.; Li, Y.; Wu, L.; Tu, Z.; Jiang, M.; Kou, Z.; Amiinu, I. S.; Mu, S. Iron-Doped Nickel Phosphide Nanosheet Arrays: An Efficient Bifunctional Electrocatalyst for Water Splitting. *ACS Appl. Mater. Interfaces* **2017**, *9* (31), 26001−26007.
(49) Jin, S. Are Metal Chalcogenides, Nitrides, and Phosphides Oxygen Evolution Catalysts or Bifunctional Catalysts? *ACS Energy Lett.* **2017**, *2* (8), 1937−1938.
(50) Song, B.; Li, K.; Yin, Y.; Wu, T.; Dang, L.; Cabán-Acevedo, M.; Han, J.; Gao, T.; Wang, X.; Zhang, Z.; Schmidt, J. R.; Xu, P.; Jin, S. Tuning Mixed Nickel Iron Phosphosulfide Nanosheet Electrocatalysts for Enhanced Hydrogen and Oxygen Evolution. *ACS Catal.* **2017**, *7* (12), 8549−8557.
(51) Xiao, P.; Chen, W.; Wang, X. A Review of Phosphide-Based Materials for Electrocatalytic Hydrogen Evolution. *Adv. Energy Mater.* **2015**, *5* (24), 1500985.
(52) Xuan, C.; Wang, J.; Xia, W.; Peng, Z.; Wu, Z.; Lei, W.; Xia, K.; Xin, H. L.; Wang, D. Porous Structured Ni−Fe−P Nanocubes Derived from a Prussian Blue Analogue as an Electrocatalyst for Efficient Overall Water Splitting. *ACS Appl. Mater. Interfaces* **2017**, *9* (31), 26134−26142.
(53) Liang, H.; Gandi, A. N.; Anjum, D. H.; Wang, X.; Schwingenschlögl, U.; Alshareef, H. N. Plasma-Assisted Synthesis of NiCoP for Efficient Overall Water Splitting. *Nano Lett.* **2016**, *16* (12), 7718−7725.
(54) Wang, A.-L.; Xu, H.; Li, G.-R. NiCoFe Layered Triple Hydroxides with Porous Structures as High-Performance Electrocatalysts for Overall Water Splitting. *ACS Energy Lett.* **2016**, *1* (2), 445−453.
(55) Nai, J.; Lu, Y.; Yu, L.; Wang, X.; Lou, X. W. Formation of Ni−Fe Mixed Diselenide Nanocages as a Superior Oxygen Evolution Electrocatalyst. *Adv. Mater.* **2017**, *29* (41), 1703870.
(56) He, W.; Wang, R.; Zhang, L.; Zhu, J.; Xiang, X.; Li, F. Enhanced photoelectrochemical water oxidation on a BiVO4 photoanode modified with multi-functional layered double hydroxide nanowalls. *J. Mater. Chem. A* **2015**, *3* (35), 17977−17982.
(57) Liu, J.; Wang, J.; Zhang, B.; Ruan, Y.; Lv, L.; Ji, X.; Xu, K.; Miao, L.; Jiang, J. Hierarchical NiCo2S4@NiFe LDH Heterostructures Supported on Nickel Foam for Enhanced Overall-Water-Splitting Activity. *ACS Appl. Mater. Interfaces* **2017**, *9* (18), 15364−15372.
(58) Zhao, Z.; Wu, H.; He, H.; Xu, X.; Jin, Y. A High-Performance Binary Ni−Co Hydroxide-based Water Oxidation Electrode with Three-Dimensional Coaxial Nanotube Array Structure. *Adv. Funct. Mater.* **2014**, *24* (29), 4698−4705.
(59) Yu, X.; Zhang, M.; Yuan, W.; Shi, G. A high-performance three-dimensional Ni-Fe layered double hydroxide/graphene electrode for water oxidation. *J. Mater. Chem. A* **2015**, *3* (13), 6921−6928.
(60) Louie, M. W.; Bell, A. T. An Investigation of Thin-Film Ni−Fe Oxide Catalysts for the Electrochemical Evolution of Oxygen. *J. Am. Chem. Soc.* **2013**, *135* (33), 12329−12337.
(61) Lee, S.; Cheon, J. Y.; Lee, W. J.; Kim, S. O.; Joo, S. H.; Park, S. Production of novel FeOOH/reduced graphene oxide hybrids and their performance as oxygen reduction reaction catalysts. *Carbon* **2014**, *80*, 127−134.
(62) Shang, C.; Dong, S.; Wang, S.; Xiao, D.; Han, P.; Wang, X.; Gu, L.; Cui, G. Coaxial NixCo2x(OH)6x/TiN Nanotube Arrays as Supercapacitor Electrodes. *ACS Nano* **2013**, *7* (6), 5430−5436.
(63) Indra, A.; Acharjya, A.; Menezes, P. W.; Merschjann, C.; Hollmann, D.; Schwarze, M.; Aktas, M.; Friedrich, A.; Lochbrunner, S.; Thomas, A.; Driess, M. Boosting Visible-Light-Driven Photocatalytic Hydrogen Evolution with an Integrated Nickel Phosphide−Carbon Nitride System. *Angew. Chem., Int. Ed.* **2017**, *56* (6), 1653−1657.
(64) Tian, J.; Liu, Q.; Asiri, A. M.; Sun, X. Self-Supported Nanoporous Cobalt Phosphide Nanowire Arrays: An Efficient 3D Hydrogen-Evolving Cathode over the Wide Range of pH 0−14. *J. Am. Chem. Soc.* **2014**, *136* (21), 7587−7590.
(65) Zhang, Y.; Ouyang, B.; Xu, J.; Jia, G.; Chen, S.; Rawat, R. S.; Fan, H. J. Rapid Synthesis of Cobalt Nitride Nanowires: Highly Efficient and Low-Cost Catalysts for Oxygen Evolution. *Angew. Chem., Int. Ed.* **2016**, *55* (30), 8670−8674.
(66) Yan, Y.; Xia, B. Y.; Ge, X.; Liu, Z.; Fisher, A.; Wang, X. A Flexible Electrode Based on Iron Phosphide Nanotubes for Overall Water Splitting. *Chem. - Eur. J.* **2015**, *21* (50), 18062−18067.
(67) Lv, C.; Peng, Z.; Zhao, Y.; Huang, Z.; Zhang, C. The hierarchical nanowires array of iron phosphide integrated on a carbon fiber paper as an effective electrocatalyst for hydrogen generation. *J. Mater. Chem. A* **2016**, *4* (4), 1454−1460.
(68) Zhai, T.; Wan, L.; Sun, S.; Chen, Q.; Sun, J.; Xia, Q.; Xia, H. Phosphate Ion Functionalized Co3O4 Ultrathin Nanosheets with Greatly Improved Surface Reactivity for High Performance Pseudocapacitors. *Adv. Mater.* **2017**, *29*, 1604167.

DOI: 10.1021/acssuschemeng.7b04808
ACS Sustainable Chem. Eng. 2018, 6, 6146−6156

(69) Zhang, R.; Wang, X.; Yu, S.; Wen, T.; Zhu, X.; Yang, F.; Sun, X.; Wang, X.; Hu, W. Ternary NiCo2Px Nanowires as pH-Universal Electrocatalysts for Highly Efficient Hydrogen Evolution Reaction. *Adv. Mater.* **2017**, *29*, 1605502.
(70) Zhang, B.; Xiao, C.; Xie, S.; Liang, J.; Chen, X.; Tang, Y. Iron−Nickel Nitride Nanostructures in Situ Grown on Surface-Redox-Etching Nickel Foam: Efficient and Ultrasustainable Electrocatalysts for Overall Water Splitting. *Chem. Mater.* **2016**, *28* (19), 6934−6941.
(71) You, B.; Sun, Y. Hierarchically Porous Nickel Sulfide Multifunctional Superstructures. *Adv. Energy Mater.* **2016**, *6*, 1502333.
(72) Tang, C.; Zhang, R.; Lu, W.; He, L.; Jiang, X.; Asiri, A. M.; Sun, X. Fe-Doped CoP Nanoarray: A Monolithic Multifunctional Catalyst for Highly Efficient Hydrogen Generation. *Adv. Mater.* **2017**, *29*, 1602441−1602446.
(73) Lu, X.; Zhao, C. Electrodeposition of hierarchically structured three-dimensional nickel−iron electrodes for efficient oxygen evolution at high current densities. *Nat. Commun.* **2015**, *6*, 6616.
(74) Li, D.; Baydoun, H.; Kulikowski, B.; Brock, S. L. Boosting the Catalytic Performance of Iron Phosphide Nanorods for the Oxygen Evolution Reaction by Incorporation of Manganese. *Chem. Mater.* **2017**, *29* (7), 3048−3054.
(75) Surendranath, Y.; Kanan, M. W.; Nocera, D. G. Mechanistic Studies of the Oxygen Evolution Reaction by a Cobalt-Phosphate Catalyst at Neutral pH. *J. Am. Chem. Soc.* **2010**, *132* (46), 16501−16509.
(76) Jin, K.; Park, J.; Lee, J.; Yang, K. D.; Pradhan, G. K.; Sim, U.; Jeong, D.; Jang, H. L.; Park, S.; Kim, D.; Sung, N.-E.; Kim, S. H.; Han, S.; Nam, K. T. Hydrated Manganese(II) Phosphate (Mn3(PO4)2·3H2O) as a Water Oxidation Catalyst. *J. Am. Chem. Soc.* **2014**, *136* (20), 7435−7443.
(77) Li, J.; Wei, G.; Zhu, Y.; Xi, Y.; Pan, X.; Ji, Y.; Zatovsky, I. V.; Han, W. Hierarchical NiCoP nanocone arrays supported on Ni foam as an efficient and stable bifunctional electrocatalyst for overall water splitting. *J. Mater. Chem. A* **2017**, *5* (28), 14828−14837.
(78) Ray, C.; Lee, S. C.; Sankar, K. V.; Jin, B.; Lee, J.; Park, J. H.; Jun, S. C. Amorphous Phosphorus-Incorporated Cobalt Molybdenum Sulfide on Carbon Cloth: An Efficient and Stable Electrocatalyst for Enhanced Overall Water Splitting over Entire pH Values. *ACS Appl. Mater. Interfaces* **2017**, *9* (43), 37739−37749.
(79) Dutta, S.; Indra, A.; Feng, Y.; Song, T.; Paik, U. Self-Supported Nickel Iron Layered Double Hydroxide-Nickel Selenide Electrocatalyst for Superior Water Splitting Activity. *ACS Appl. Mater. Interfaces* **2017**, *9* (39), 33766−33774.
(80) Chen, G.-F.; Ma, T. Y.; Liu, Z.-Q.; Li, N.; Su, Y.-Z.; Davey, K.; Qiao, S.-Z. Efficient and Stable Bifunctional Electrocatalysts Ni/NixMy (M = P, S) for Overall Water Splitting. *Adv. Funct. Mater.* **2016**, *26* (19), 3314−3323.
(81) Huang, H.; Yu, C.; Zhao, C.; Han, X.; Yang, J.; Liu, Z.; Li, S.; Zhang, M.; Qiu, J. Iron-tuned Super Nickel Phosphide Microstructures with High Activity for Electrochemical Overall Water Splitting. *Nano Energy* **2017**, *34*, 472−480.
(82) Li, Y.; Zhang, H.; Jiang, M.; Kuang, Y.; Sun, X.; Duan, X. Ternary NiCoP nanosheet arrays: An excellent bifunctional catalyst for alkaline overall water splitting. *Nano Res.* **2016**, *9* (8), 2251−2259.
(83) Li, J.; Yan, M.; Zhou, X.; Huang, Z. Q.; Xai, Z.; Chang, C. R.; Ma, Y.; Qu, Y. Mechanistic Insights on Ternary $Ni_{2-x}CoxP$ for Hydrogen Evolution and Their Hybrids with Graphene as Highly Efficient and Robust Catalysts for Overall Water Splitting. *Adv. Funct. Mater.* **2016**, *26* (37), 6785−6796.
(84) Yu, J.; Li, Q. Q.; Li, Y.; Xu, C. Y.; Zhen, L.; Dravid, V. P.; Wu, J. S. Ternary Metal Phosphide with Triple-Layered Structure as a Low-Cost and Efficient Electrocatalyst for Bifunctional Water Splitting. *Adv. Funct. Mater.* **2016**, *26* (42), 7644−7651.
(85) Wei, L.; Goh, K.; Birer, O.; Karahan, H. E.; Chang, J.; Zhai, S.; Chen, X.; Chen, Y. A hierarchically porous nickel−copper phosphide nano-foam for efficient electrochemical splitting of water. *Nanoscale* **2017**, *9* (13), 4401−4408.
(86) Yan, L.; Cao, L.; Dai, P.; Gu, X.; Liu, D.; Li, L.; Wang, Y.; Zhao, X. Metal-Organic Frameworks Derived Nanotube of Nickel-Cobalt Bimetal Phosphides as Highly Efficient Electrocatalysts for Overall Water Splitting. *Adv. Funct. Mater.* **2017**, *27* (40), 1703455.
(87) Zhu, X.; Tang, C.; Wang, H.-F.; Li, B.-Q.; Zhang, Q.; Li, C.; Yang, C.; Wei, F. Monolithic-structured ternary hydroxides as freestanding bifunctional electrocatalysts for overall water splitting. *J. Mater. Chem. A* **2016**, *4* (19), 7245−7250.
(88) Du, C.; Shang, M.; Mao, J.; Song, W. Hierarchical MoP/Ni2P heterostructures on nickel foam for efficient water splitting. *J. Mater. Chem. A* **2017**, *5* (30), 15940−15949.

DOI: 10.1021/acssuschemeng.7b04808
ACS Sustainable Chem. Eng. 2018, 6, 6146−6156